COMMUNICATION

Encapsulation of shear thickening fluid as an easy-to-apply impact-resistant material†

He Zhang, ‡[ab] Xin Zhang,‡[ce] Qian Chen,[d] Xin Li,[b] Pengfei Wang,[d] En-Hua Yang,[e] Fei Duan,[b] Xinglong Gong, [d] Zhong Zhang [f] and Jinglei Yang*[g]

In this investigation, a hard-to-handle shear thickening fluid (STF) is successfully encapsulated for easy handling and re-processing. The encapsulated STF is a promising impact-resistant material. Double-walled macroscopic STF capsules are synthesized using a convenient process by instilling diluted STF droplets into reaction solution. The obtained STF capsules show good shear thickening response to dynamic impact in comparison to quasi-static compression (154 times higher absorbed nominal strain energy). The capsules' robustness and capacity to absorb impact energy can be adjusted by varying the reaction time and the amount of chloroform in the reaction solution. This innovative method opens a new window to design and manufacture versatile impact-resistant materials and structures.

Materials with good impact resistance are increasingly demanded to ensure the safety of personnel or equipment at a risk of encountering impacts in scenarios ranging from military settings (*e.g.*, body armor, armored vehicles, and protective bastions) to civilian ones (*e.g.*, sports equipment, motor vehicles, and sophisticated but delicate electronic devices).[1] Tremendous efforts have been put into investigations on how to improve the impact resistance of materials. For example, superior impact-resistant biomimetic composites with hierarchical multi-scaled structures similar to nacre were recently synthesized artificially by first studying natural objects and then using reverse engineering to reproduce the hierarchical structures.[2]

In addition to the primary consideration of impact resistance, in some cases (*e.g.*, bullet/stab-proof clothing as body armor and kneepads as protective sports equipment), it is also necessary for the material to balance flexibility to allow normal body movements and protectiveness against accidental low-speed and high-speed impacts. Shear thickening fluid (STF), a non-Newtonian liquid whose viscosity increases rapidly with increasing shear rate, especially after a threshold shear rate,[3–5] can deliver this balance as a unique impact-resistant material.[6–8] However, the practical applications of STF are restricted by its physical and chemical properties, which include high viscosity, hygroscopicity, and difficulty in handling or integrating into structures. To overcome these disadvantages and increase the stability of STF during its service life, it is important to explore techniques for packaging this highly viscous fluid.

Investigations have focused on resolving or partially resolving this challenge. For example, the STF alone or fabrics impregnated with STF can be packaged and sealed using polyethylene film to minimize the external influence from the surroundings.[9–11] To incorporate STF into polymer composites, other porous structures such as foam, cellular solids, fibrous matrices, and scaffolds[12,13] have been adopted to carry and reserve STF in the composites. In a patented work,[13] STF spheres were directly generated in a rubber matrix by first emulsifying STF in immiscible rubber precursors and then converting the precursors to a solid through chemical reaction. While these approaches solve the problem caused by the external environment, they cannot eliminate the mutual interactions between STF and the fabrics or polymers. Complexes with STF cores enclosed by thermoplastic polymer tubes have also been fabricated using a co-extruding method.[14] However, the reprocessing of this core–shell tubular structure into various matrices remains challenging.

aSouth China University of Technology, National Engineering Research Center of Novel Equipment for Polymer Processing, Ministry of Education, Key Laboratory Polymer Processing Engineering, Guangzhou 510641, China

bSchool of Mechanical and Aerospace Engineering, Nanyang Technological University, Singapore, 639798, Singapore

cInterdisciplinary Graduate School, Nanyang Technological University, 50 Nanyang Avenue, Singapore, 639798, Singapore

dCAS Key Laboratory of Mechanical Behavior and Design of Materials, University of Science and Technology of China (USTC), Hefei 230027, China

eSchool of Civil and Environmental Engineering, Nanyang Technological University, Singapore, 639798, Singapore

fCAS Key Laboratory of Nanosystem and Hierarchical Fabrication, National Center for Nanoscience and Technology, Beijing 100190, China

gDepartment of Mechanical and Aerospace Engineering, Hong Kong University of Science and Technology, Clear Water Bay, Kowloon, Hong Kong SAR, China. E-mail: maeyang@ust.hk

† Electronic supplementary information (ESI) available. See DOI: 10.1039/c7ta04904h

‡ He Zhang and Xin Zhang contributed equally to this work.

22472 | *J. Mater. Chem. A*, 2017, 5, 22472–22479

This journal is © The Royal Society of Chemistry 2017

To completely overcome the above-mentioned disadvantages and increase the stability of STF during its service life, it is of great significance to explore techniques to tightly package this highly viscous fluid. Encapsulation is among the most promising techniques to achieve this because it can not only solidify the STF for easy handling, but also isolate it to minimize the influence of the surrounding environment.[15–22] However, due to the high viscosity of STF, the shear thickening effect, and the multiple ingredients of STF,[23,24] the encapsulation of STF represents a significant challenge. Although numerous techniques have been demonstrated for the encapsulation of solids and liquids with relatively low viscosities,[25–28] until now, no investigations have been reported on the encapsulation of liquids with high viscosity like STF.

In this study, a convenient and simple method for the encapsulation of STF is proposed. STF droplets are generated using a syringe, and the droplets are then instilled in reaction solution in a container for encapsulation under shaking at room temperature (Fig. 1a). After being diluted to 85 wt% (STF-85) with 5 wt% polyethyleneimine (PEI) with a molecular weight of about 600 and 10 wt% ethane diol (EDO) as diluent, STF is loaded into a syringe with a needle to generate droplets. The reaction solution in the container is a mixture of 4.0 g diisocyanate prepolymer, Suprasec 2644, 6.0 ml toluene as the major solvent, and variable amounts of chloroform to adjust the density and the polarity of the solution. To better generate spherical droplets in the solution, about 1.5–2.0 ml toluene is gently added dropwise to the surface of the mixture to form a density gradient after the formation of a uniform mixture. With the needle located about 3–4 cm above the reaction solution, the STF in the syringe was slowly added into the reaction solution in the form of individual droplets. When the instilled STF droplets contact the reaction solution, the PEI diffuses across the interface and reacts with Suprasec 2644, as schematically shown in Fig. S1,† to form the preliminary polyurea membrane to enwrap the droplet. To obtain uniform growth of the shell, the droplets are then gently shaken using a shaker in the reaction solution for different durations ranging from 5 to 180 min.

The STF adopted in the encapsulation process consists of poly(styrene-*alt*-ethyl acrylate) [P(St-EA)] as the hard nanoparticles and EDO as the suspension medium. Fig. S2 and S3† show the morphology and size distribution of the P(St-EA) nanoparticles in the STF, respectively. Almost all the nanoparticles are spherical, and their diameters are quite uniform, ranging from 330 to 410 nm with an average of 377 ± 34 nm. Due to the adoption of EDO rather than some other poly(ethylene glycol), the STF used in this study has a relatively low initial viscosity (∼8Pa s, as shown in Fig. S4†), which is beneficial to the encapsulation process. However, the original STF still cannot be extruded through the small needle without dilution because of the relatively high initial viscosity and the shear thickening effect. Fig. S4† shows the rheological behaviors of the original STF and STF-85. The usage of EDO as a diluent dramatically decreases the viscosity of the STF to about 0.6 Pa s and eliminates the shear thickening effect without increasing the complexity of the mixture by adding new ingredients. The compositions of the original STF, STF-85, pure PEI, and pure EDO were analyzed by thermogravimetric analysis (TGA), as shown in Fig. S5.† The weight percentage of the nanoparticles in the original STF is about 50 wt%.
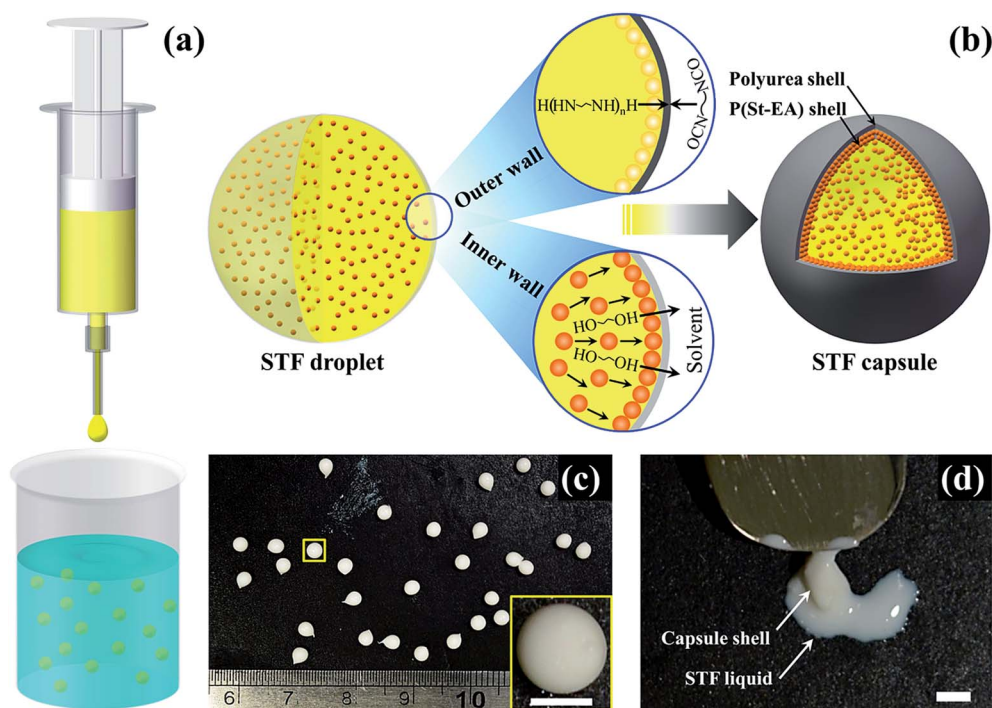

Fig. 1 (a) Schematic showing the setup for STF encapsulation (not to scale). (b) Schematic showing the formation mechanism of the outer and inner walls of the STF capsule (not to scale). (c) Optical image of the obtained STF-85 capsules with one enlarged in the inset. (d) A broken STF-85 capsule. The capsules in (c and d) were obtained with a reaction time of 60 min in RS-5.7. The scale bars in the inset of (c and d) represent 2 mm.

Macroscopic STF capsules can be successfully synthesized by the proposed simple device and simple process. Fig. 1c shows an optical image of STF-85 capsules synthesized in reaction solution containing 5.7 ml chloroform (RS-5.7) for 60 min. The capsule in the yellow frame in Fig. 1c is enlarged in the inset to show the general appearance. The capsules are dry and flow-free, indicating that there is no leakage of the encapsulated core liquid after the encapsulation process. In addition to the perfect spherical shapes observed of most capsules, some irregular shapes are also found, as illustrated schematically in Fig. S6.† The different shapes result from the instability of the density gradient generated by the late addition of 1.5–2.0 ml toluene because the density gradient changes gradually due to the interdiffusion of the ingredients in the reaction solution and the disturbance caused by the instilled STF droplets. Based on the measurement of more than 50 individual capsules, the average diameter of the capsules is 2.7 ± 0.2 mm, much larger than those of microcapsules obtained using traditional encapsulation techniques.[18,29,30] Breaking one STF capsule with a steel plate indicated that a large amount of liquid was contained inside the capsule, as shown in Fig. 1d.

The microscopic structures of the STF-85 capsules were observed using field-emission scanning electronic microscopy (FESEM). As above, the imaged STF-85 capsules were synthesized in RS-5.7 with a reaction time of 60 min. As shown in Fig. 2a, the capsule has a very smooth outer surface, quite similar to the polyurea walls of the microcapsules obtained by Sun et al.[31,32] Due to the high cross-linking density of the formed polyurea walls introduced by the large amount of reactive hydrogen atoms in PEI, the outer walls are very dense without any visible pores under high-resolution SEM imaging (Fig. S7†). According to Sun et al.,[31,32] the polyurea shells of microcapsules synthesized with ethylenimines (e.g., triethylenetetramine and tetraethylenepentamine) have superior impermeability towards both water and some organic solvents due to the highly cross-linked, dense structure. This is very important to keep the STF inside the capsules since it protects the STF from the surrounding environment. Uniform wrinkles and minor shrinkage can be observed on the capsule, which is characteristic of most capsules synthesized by interfacial polymerization due to the diffusion of core substances during the formation of the capsule shell. Although the STF capsules in this study are much larger (several millimeters) than other polyurea microcapsules (micron level) and lose more core substance due to the diffusion and dissolution of EDO in the external solvent, the level of shrinkage is much smaller than in most polyurea microcapsules.[31] Fig. 2b shows the cross section of a typical capsule. The imaged sample was prepared by cutting the capsule using a sharp blade followed by washing away the core mixture. As can be seen in Fig. S8a,† the shell retains its original shape after the removal of the inside core, demonstrating the rigidity and robustness of the shell. Compared to the total diameter of the capsule (about 2.7 mm), the thickness of the shell (about 100 μm) means that there is a big chamber that can reserve a large amount of STF inside. Fig. 2e shows the trend in shell thickness measured from the cross sections of STF-85 capsules obtained with different reaction times of 30, 60, and

120 in RS-5.7 (Fig. S9†). The shell thickness increased with increasing reaction time, indicating that more robust capsules can be obtained with longer reaction time. Interestingly, the shell has a double-walled structure (Fig. 2b), and the outer wall can be totally peeled away from the inner wall, as indicated by the arrow in Fig. S8b.† The cross section in the white frame in Fig. 2b is enlarged in Fig. 2c and d, showing that the inner wall is composed of closely packed P(St-EA) nanoparticles (Fig. 2c), while the outer wall consists of a dense membrane decorated with irregularly distributed P(St-EA) nanoparticles (Fig. 2d). It can be concluded that the robustness of the STF capsule results from both the tightness of the dense outer polyurea wall and the thick inner wall of agglomerated nanoparticles.

The proposed mechanism of shell formation is illustrated in Fig. 1b. Upon instillation of the diluted STF into the reaction solution, the PEI near the interface between the STF droplet and reaction solution immediately diffuses across the interface and reacts with Suprasec 2644, which is attributed to the extremely high reactivity between isocyanate and amine. Preliminary polyurea walls form around the droplets to protect them from collapse and reduce the interdiffusion of ingredients between the core and the reaction solution. Although EDO is insoluble in toluene, it is partially miscible with chloroform.[33] With increasing immersion time in the reaction solution, EDO gradually diffuses through the interface or the formed wall to either dissolve in the reaction solution or react with Suprasec 2644 to generate polyurethane and thicken the outer shell. Accompanying the diffused EDO, the P(St-EA) nanoparticles migrate to the interface due to their high affinity for toluene and especially chloroform in the reaction solution. Because of the formed shell, the nanoparticles can only concentrate and adhere to the inner side of the polyurea wall, resulting in the formation of a thick inner wall. This step is necessary to form robust STF capsules considering that the generated STF droplets have sizes of up to several millimeters, while the maximum thickness of the formed polyurea shell is only several microns or several tens of microns. The influence of the solvent on the P(St-EA) nanoparticles inside the capsule was minimized by the outer polyurea wall. After being immersed in the reaction solution for 60 min, the nanoparticle morphology does not change perceptibly, and the diameter only slightly increases from 377 ± 34 nm to 380 ± 25 nm (Fig. 2c and d).

This proposed mechanism was verified by two control experiments in this investigation. To determine the function of PEI, diluted STF without the PEI was used in the encapsulation process. The STF without the addition of PEI is not able to be encapsulated completely. The STF droplets split into small debris during the shaking process. Without the protection of the preliminary polyurea membrane, the P(St-EA) nanoparticles easily swell or even dissolve in the solvent from the reaction solution. Fig. S10† shows the P(St-EA) nanoparticles in STF droplets after being immersed in the reaction solution without Suprasec 2644 for 5, 30, 60, and 120 min. The nanoparticles were gradually swollen by the solvent (Fig. S11†), and a polymeric network resembling a loofah sponge formed at the interface between the STF droplet and the solvent after 60 min (Fig. S10d and e†). Some very large P(St-EA) nanoparticles with

22474 | J. Mater. Chem. A, 2017, 5, 22472–22479

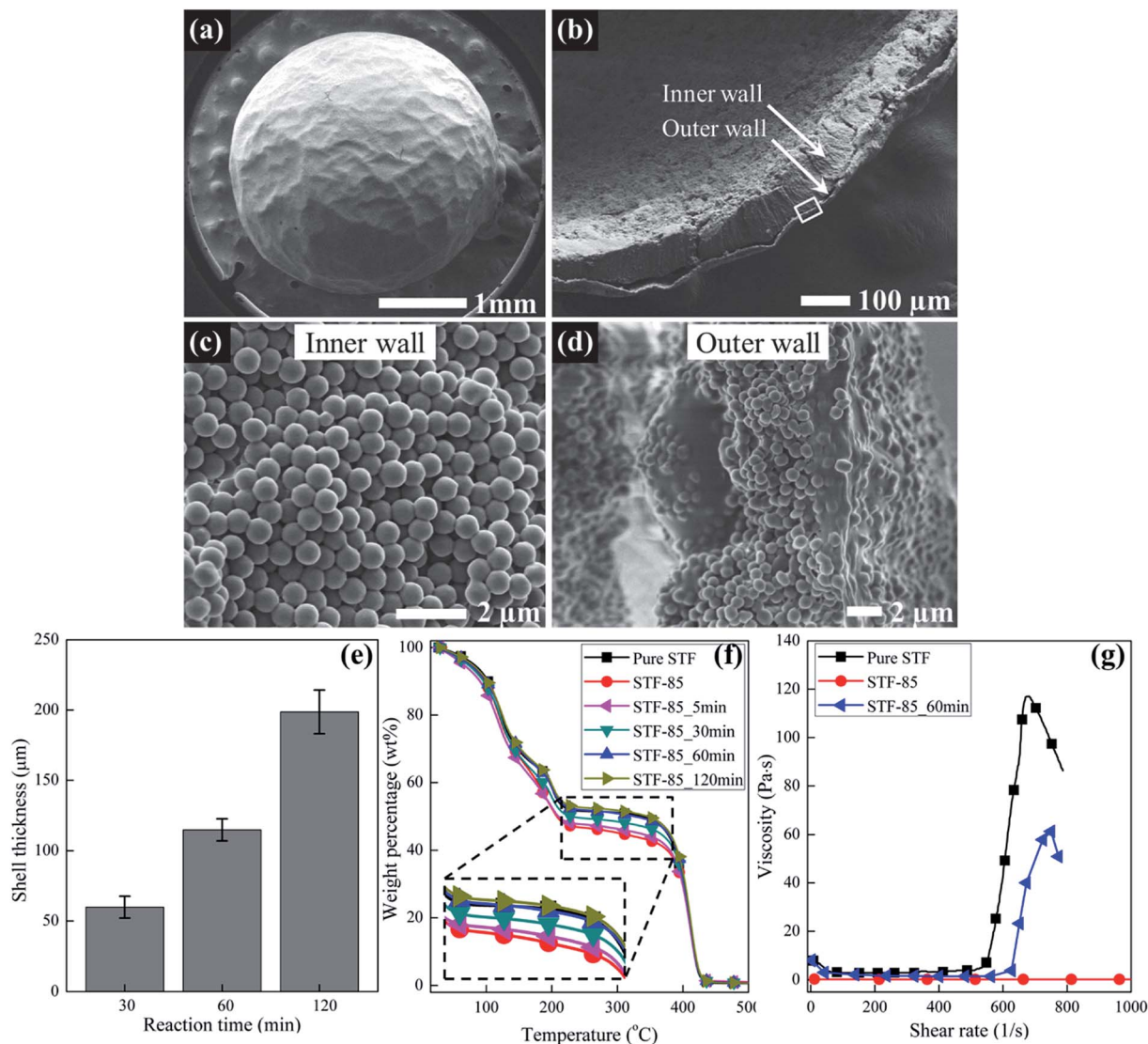This journal is © The Royal Society of Chemistry 2017

Fig. 2 Characterization of the formed STF-85 capsules: (a) a single STF-85 capsule with a smooth outer polyurea membrane; (b) double-walled structure of the cross section of a manually broken STF-85 capsule; (c) inner wall of the STF-85 capsule; (d) outer wall of the STF-85 capsule; (e) trend in shell thickness with respect to reaction time in RS-5.7; (f) TGA curves of the cores squeezed from STF-85 capsules formed with different reaction times in RS-5.7; and (g) rheological behavior of the original STF, input STF-85 before encapsulation, and the core mixture squeezed from STF-85 capsules with a reaction time of 60 min in RS-5.7.

diameters of up to 1 μm were observed after the droplets were immersed in the solvent for 120 min (Fig. S10f†). This demonstrates that the formation of the polyurea shell is critical to protect the liquid core inside. To verify that the inner shell of agglomerated nanoparticles support the large STF capsules, another STF based on a silica nanoparticle suspension in EDO was used for encapsulation *via* the same process. Although thin outer shells formed around the STF droplets, the silica nanoparticles did not agglomerate on the inner side of the polyurea wall due to the low affinity between inorganic silica and the solvent in the reaction solution. Thus, no robust capsules were formed regardless of the reaction time.

It can be seen that chloroform plays a key role in the reaction solution during the encapsulation process. The function of chloroform in the reaction solution is three-fold. First, due to

the relatively high density (1.492 g ml^{-1} at 25 °C) of chloroform compared to the main solvent toluene (0.865 g ml^{-1} at 25 °C), it can adjust the density of the reaction solution to match that of the diluted STF. In this situation, the generated STF droplets are suspended in the reaction solution instead of flowing to the top or precipitating to the bottom, resulting in the formation of a uniform shell. In addition, because it is partially miscible with EDO, the chloroform can gradually dissolve the excess EDO in the diluted STF to increase the volume fraction of suspended nanoparticles in the core mixture after the encapsulation process. Finally, because of its affinity for the P(St-EA) nanoparticles, chloroform can attract, swell, or even dissolve the nanoparticles to form the inner wall of the STF capsule.

After the successful fabrication of the STF capsules, mechanical tests, including quasi-static compression and low-

speed impact tests, were conducted to study the properties of the obtained capsules using devices schematically shown in Fig. S12a and b.† Fig. 3a shows the typical curves of nominal stress *versus* nominal strain for the quasi-static compression of single STF-85 capsules obtained in RS-5.7 with different reaction times. Fig. S14–S16† show the trends in maximum nominal strain, nominal strength, and nominal elastic modulus, respectively. All three of these parameters increases with increasing reaction time, consistent with the trend in shell thickness shown in Fig. 2e.

Fig. 3b shows the typical stress *versus* nominal strain curves under dynamic loading for the same STF-85 capsule. The maximum detected stress decreases with increasing reaction time from 5 to 120 min. For STF-85 capsules with a reaction time of 5 min, stress was not detected during the early stage of the impact process. Subsequently, stress sharply increases to its peak value within a very short time at the end of the impact process. The high-speed camera images show that before reaching the peak stress value, STF was squeezed out and sprayed like a normal viscous liquid, as shown in Video S1.† This means there is no shear thickening effect for the encapsulated STF with a reaction time of 5 min, and the sharp increase in stress is attributed to the direct pressing of the

sensor by the impactor after capsule failure. Upon increasing the reaction time to 30, 60, and finally 120 min, the maximum stress decreases, while the width of the peak increases dramatically, and the stress is detected sooner after the impactor makes contact with the capsule. The STF-85 capsules obtained with reaction time of 180 min in RS-5.7 were also subjected to dynamic impact test, as shown in Fig. 3b. It can be seen that the maximum nominal stress increases again. The increase can be attributed to the solidification of the liquid core, as shown in Fig. S17,† due to the excessive diffusion of the EDO medium and the swelling of the P(St-EA) nanoparticles during the long reaction time. By comparing the curves of the STF capsules with different reaction times, it can be seen that the liquid STF-85 capsules with reaction time of 60 and 120 min behave more like the solidified STF capsules with reaction time of 180 min under impact loading.

Fig. 3c shows the absorbed nominal strain energy (E_n) of STF-85 capsules with respect to reaction time under both quasi-static and dynamic loading. The ratio of absorbed energy under dynamic impact to quasi-static compression is also shown. The nominal strain energy under quasi-static loading is integrated until catastrophic failure of the tested capsule. In contrast, the nominal strain energy under dynamic impact is
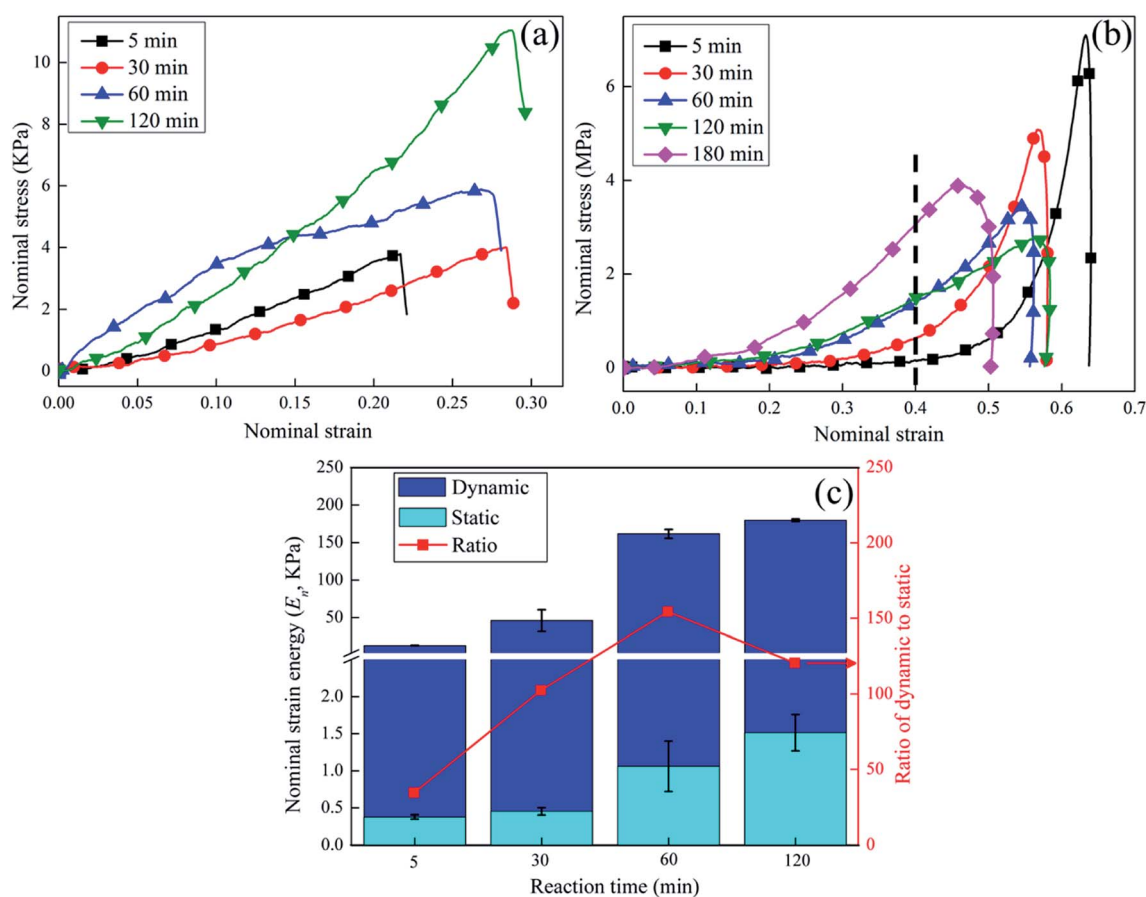

Fig. 3 Mechanical response of a single STF-85 capsule under quasi-static compression and dynamic impact: (a) typical curve of nominal stress *versus* nominal strain under quasi-static compressive loading; (b) typical stress *versus* nominal strain curve under dynamic loading; and (c) comparison of the absorbed nominal strain energy for the STF-85 capsule with respect to reaction time under quasi-static compression and dynamic impact.
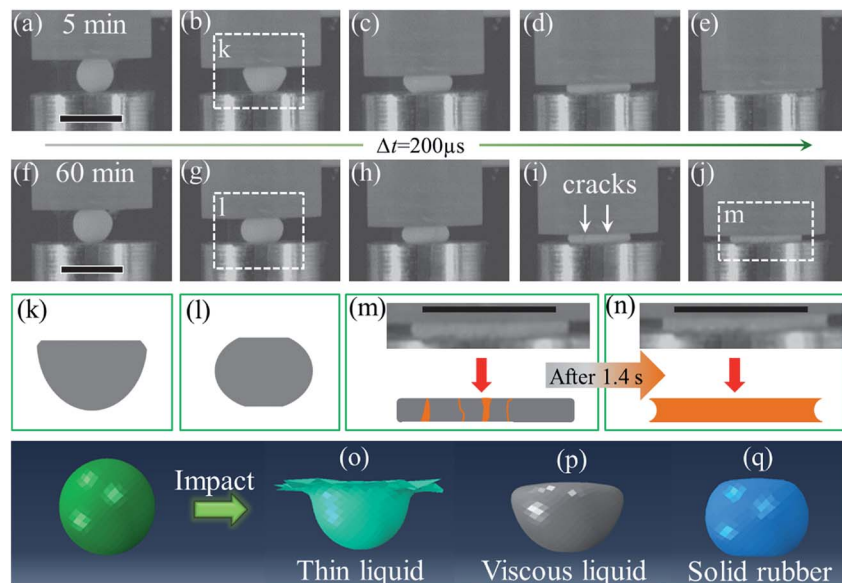
22476 | *J. Mater. Chem. A*, 2017, **5**, 22472–22479

This journal is © The Royal Society of Chemistry 2017

Fig. 4 Response of STF-85 capsules under impact loading. (a–e) and (f–j) digital images collected by a high-speed camera with a time interval of 200 μs to reveal the impact behavior of STF-85 capsules with reaction times of 5 and 60 min in RS-5.7, respectively. (k and l) schematic shapes of STF-85 capsules with reaction times of 5 and 60 min in RS-5.7 at the early stage of impact (∼200 μs), as observed by high-speed camera. (m and n) flow behavior of the core liquid in a STF-85 capsule obtained with a reaction time of 60 min in RS-5.7 at the end of the impact (∼800 μs) and after impact (∼1.4 s). (o–q) Deformation simulated by finite element method for different materials under impact at 200 μs: pure water with a viscosity of 0.89 mPa s (o); pure glycerol with a viscosity of 1.4 Pa s (p); and solid rubber with an elastic modulus of 10 MPa (q). The scale bars in (a–e), (f–j), (m), and (n) represent 5 mm.

integrated until the strain reaches 0.4 (before the vertical dashed line in Fig. 3b) since it is impossible to identify catastrophic failure under dynamic impact. The absorbed strain energy during both tests increases with increasing reaction time, and the absorbed strain energy under dynamic impact is much higher than that under quasi-static compression; the ratio between them increases from about 34 for a reaction time of 5 min to about 154 for a reaction time of 60 min and then decreases to about 120 for a reaction time of 120 min. Although the ratio of the absorbed strain energy between the quasi-static and dynamic tests indicates a loading rate effect during the impact process,[34] the rapid increase of the ratio and the trend in the ratio with peak at a reaction time of 60 min suggest that the shear thickening effect of the core liquid may play a significant role during the impact process to absorb more strain energy.

Direct evidence of the shear thickening effect was obtained by studying the encapsulated core mixture alone. The core mixtures of STF-85 capsules were extracted and subjected to TGA and rheological testing to characterize the core composition and rheological behavior, respectively. Fig. 2f shows the TGA curves of the squeezed cores from STF-85 capsules obtained in RS-5.7 with reaction times ranging from 5 to 120 min. The volume fraction of the suspended P(St-EA) nanoparticles in the core liquid gradually approaches that of the original STF with increasing reaction time from 5 to 60 min and finally exceeds that of the original STF at a reaction time of 120 min. Fig. 2g compares the rheological behavior of the core squeezed from STF-85 capsules formed with a reaction time of 60 min in RS-5.7 to those of the original STF and the input STF-85 for

encapsulation. A shear thickening effect can be observed for the squeezed core mixture. However, this effect is not as strong as the effect observed for the original STF. This discrepancy may be attributed to the volume fraction of the suspended nanoparticles in the core of the STF-85 capsules obtained with a reaction time of 60 min, which deviates slightly from that of the original STF. Another possible explanation is that the STF used in the rheological test absorbs moisture from the surroundings during preparation, which involved the squeezing of more than 60 capsules. Nevertheless, the results directly verify the shear thickening effect of the encapsulated STF after the encapsulation process.

The impact process was also recorded by high-speed camera to investigate the impact behavior of the STF-85 capsules obtained with reaction times of 5 and 60 min in RS-5.7, as respectively shown in Videos S1 and S2. Fig. 4a–e and f–j respectively show the freeze frames of the two videos with time intervals of 200 μs to reveal the deformation and failure processes of the capsules. As shown in Fig. 4b (reaction time = 5 min) and the corresponding schematic illustration in Fig. 4k, a shape similar to a conical frustum was observed during the early stage (∼200 μs) of the impact process, indicating non-homogeneous deformation. However, for the STF-85 capsule with a reaction time of 60 min in RS-5.7, a shape similar to a Chinese drum was observed in the same impact test, indicating homogeneous deformation (Fig. 4g and the schematic illustration in Fig. 4l). The deformation of the STF capsule is similar to that of an elastic golf ball hitting a steel target.[35] This indicates that the STF capsule comes to an equilibrium state

immediately during impact, suggesting that the encapsulated STF transfers from a liquid to a solid during the impact process.

As can be seen in Video S2† and the freeze frame in Fig. 4i, quite a few cracks (indicated by the arrows in Fig. 4i) appear during the impact process, and the STF inside remains solid rather than being squeezed and sprayed out like a liquid, as shown in Video S1.† However, after 1.4 s, this solid material finally turns to liquid and covers the damaged sample, as illustrated by the increased light reflection from the light-emitting diode of the high-speed camera (Fig. 4n). Moreover, in contrast to the raised curve of the damaged sample between the impactor and holder right after the impact process (Fig. 4m), a hyperbolic contour of the damaged sample was observed after 1.4 s (Fig. 4n). This indicates that the leaked STF from the capsule turns to liquid to wet the surface of the damaged sample and forms the observed shape due to the capillary effect in the small gap. The phenomenon captured by the high-speed camera is consistent with the behavior recorded by the stress–strain curves, which both demonstrate the effectiveness of shear thickening in the STF after encapsulation. The reversible change in the encapsulated STF from liquid to solid upon dynamic impact and from solid to liquid after the impact process means that the encapsulation process does not influence the behavior of the nanoparticles in STF.

The deformation pattern of a spherical material with a diameter of 2.7 mm under similar initial impact velocity (about 3 m s^{-1}) and energy as in the experiment was studied by finite element analysis using Abaqus/Explicit. Three different materials [pure water (thin liquid) with a viscosity of 0.89 mPa s; glycerol (viscous liquid) with a viscosity of 1.4 Pa s; and rubber (solid material) with an elastic modulus of 10 MPa] were simulated for comparison. Fig. 4o–q show the simulated response of the three different materials upon impact. The results indicate that non-homogeneous deformation occurs for liquids like water and glycerol, while an equilibrium state is reached for rubber. Meanwhile, the thinner liquid (i.e., water) shows much more severe non-homogeneous deformation compared to the viscous liquid (i.e., glycerol). The consistency between the experiment and simulation suggests that the STF

capsules fabricated with a reaction time of 60 min show a good shear thickening effect and behave like a solid during impact, while the capsules formed with a reaction time of 5 min still behave like a liquid.

The above experiments show that the reaction time is a key parameter in the encapsulation process in RS-5.7 to achieve STF-85 capsules with shear thickening effect. As mentioned previously, chloroform also plays an important role in the encapsulation process to control the volume fraction of suspended nanoparticles in the core mixture of the capsules. Because of this, STF-85 capsules synthesized in other reaction solutions with different amounts of chloroform [3.7 ml (RS-3.7), 4.7 ml (RS-4.7), and 6.7 ml (RS-6.7)] with other conditions kept the same were also subjected to mechanical tests. Fig. 5a and b respectively show the nominal strength under quasi-static compression and absorbed nominal strain energy under dynamic impact of the STF capsules obtained from the reaction solutions with different reaction durations. Both the nominal strength and the absorbed nominal strain energy increase with increasing reaction time in the same reaction solution. In addition, for the same reaction time, a larger amount of chloroform is beneficial for the formation of better STF capsules in terms of both nominal strength and absorbed nominal strain energy. In RS-3.7 with less chloroform, no robust STF capsules are obtained at the reaction times of 5 and 30 min. Although a longer reaction time can generate robust STF capsules, it also results in the swelling of the P(St-EA) nanoparticles, which may affect the shear thickening effect, as indicated by the much lower absorbed strain energy of the STF capsules obtained at 180 min in RS-3.7 (Fig. 5b). However, too much chloroform in RS-6.7 is also undesirable because (1) all the droplets float on the surface of the reaction solution, affecting the formation of a uniform shell because of the density mismatch, and (2) the large amount of chloroform leads to the rapid solidification of the capsule core due to the faster diffusion of EDO and the weaker shell because of the shorter time available for shell formation. Consequently, STF-85 capsules obtained in RS-6.7 were not investigated in this study. Based on these observations, the reaction solution with 5.7 ml chloroform (RS-5.7) is the most suitable mixture for the generation of STF capsules.
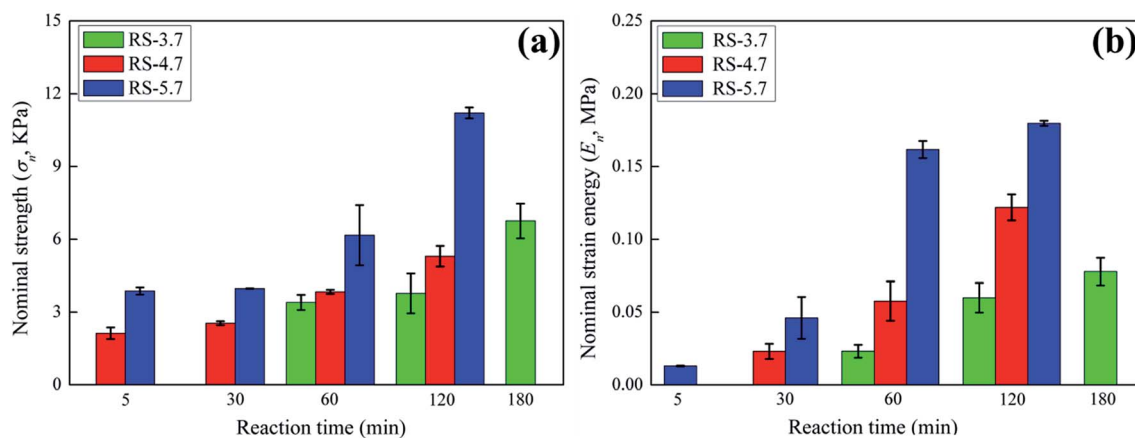

Fig. 5 Effect of the amount of chloroform in the reaction solution on the mechanical behavior of STF-85 capsules obtained from RS-3.7, RS-4.7, and RS-5.7 in different reaction times: (a) nominal strength under quasi-static compression and (b) absorbed nominal strain energy.

22478 | J. Mater. Chem. A, 2017, 5, 22472–22479

This journal is © The Royal Society of Chemistry 2017

In summary, macroscopic STF capsules possessing good shear thickening effect were successfully synthesized using a simple process by instilling diluted STF droplets into a reaction solution. Double-walled shells were formed; outer polyurea walls were generated as a result of the interfacial reaction between the PEI diffused from the core and the diisocyanate pre-polymer, and the inner walls consisted of deposited P(St-EA) nanoparticles. The thin and dense outer wall imparts impermeability to the shell, while the thick inner wall provides a strong support for the large capsule. The chloroform plays an key role in the reaction solution during the encapsulation process because it can adjust the density and polarity of the reaction solution, dissolve excess EDO from the diluted STF, and attract the P(St-EA) nanoparticles to deposit on the shell. A much higher strain energy can be absorbed under dynamic impact loading compared to quasi-static compression loading, indicating that the STF after encapsulation retains the shear thickening effect to absorb the impact energy. The properties of the STF capsules can be tuned by the reaction time and the amount of chloroform added to the reaction solution. The encapsulation technique used to produce STF capsules with high robustness and ability to absorb strain energy provides a new way to design and manufacture versatile impact-resistant materials and structures.

Conflicts of interest

The authors declare no conflicts of interest.

Acknowledgements

References

1 S. Wang, S. Xuan, W. Jiang, W. Jiang, L. Yan, Y. Mao, M. Liu and X. Gong, *J. Mater. Chem. A*, 2015, **3**, 19790–19799.

2 J. B. Thompson, J. H. Kindt, B. Drake, H. G. Hansma, D. E. Morse and P. K. Hansma, *Nature*, 2001, **414**, 773–776.

3 N. J. Wagner and J. F. Brady, *Phys. Today*, 2009, **62**, 27–32.

4 E. Brown, N. A. Forman, C. S. Orellana, H. J. Zhang, B. W. Maynor, D. E. Betts, J. M. DeSimone and H. M. Jaeger, *Nat. Mater.*, 2010, **9**, 220–224.

5 W. J. Wen, X. X. Huang, S. H. Yang, K. Q. Lu and P. Sheng, *Nat. Mater.*, 2003, **2**, 727–730.

6 T. A. Hassan, V. K. Rangari and S. Jeelani, *Mater. Sci. Eng., A*, 2010, **527**, 2892–2899.

7 A. Majumdar, B. S. Butola and A. Srivastava, *Mater. Des.*, 2014, **54**, 295–300.

8 A. Haris, H. P. Lee, T. E. Tay and V. B. C. Tan, *International Journal of Impact Engineering*, 2015, **80**, 143–151.

9 Y. S. Lee, E. D. Wetzel and N. J. Wagner, *J. Mater. Sci.*, 2003, **38**, 2825–2833.

10 M. J. Decker, C. J. Halbach, C. H. Nam, N. J. Wagner and E. D. Wetzel, *Compos. Sci. Technol.*, 2007, **67**, 565–578.

11 J. N. Fowler, A. A. Pallanta, C. B. Swanik and N. J. Wagner, *J. Biomech. Eng.*, 2015, **137**, 054504.

12 S. S. Deshmukh and G. H. Mckinley, *US Pat.*, 20040173422, 2004.

13 N. J. Wagner, J. E. Kirkwood and R. G. Egres Jr, *US Pat.*, 20060234572, 2006.

14 R. B. Borella, R. P. Barry, T. T. Allgeuer and H. H. Den, WO 2008115636 A1, 2008.

15 S. R. White, N. R. Sottos, P. H. Geubelle, J. S. Moore, M. R. Kessler, S. R. Sriram, E. N. Brown and S. Viswanathan, *Nature*, 2001, **409**, 794–797.

16 M. M. Caruso, B. J. Blaiszik, H. Jin, S. R. Schelkopf, D. S. Stradley, N. R. Sottos, S. R. White and J. S. Moore, *ACS Appl. Mater. Interfaces*, 2010, **2**, 1195–1199.

17 M. Huang and J. Yang, *J. Mater. Chem.*, 2011, **21**, 11123–11130.

18 B. J. Blaiszik, S. L. B. Kramer, M. E. Grady, D. A. McIlroy, J. S. Moore, N. R. Sottos and S. R. White, *Adv. Mater.*, 2012, **24**, 398–401.

19 H. Jin, C. L. Mangun, D. S. Stradley, J. S. Moore, N. R. Sottos and S. R. White, *Polymer*, 2012, **53**, 581–587.

20 H. Zhang and J. Yang, *J. Mater. Chem. A*, 2013, **1**, 12715–12720.

21 Y. Zheng, Z. Y. Yu, R. M. Parker, Y. C. Wu, C. Abell and O. A. Scherman, *Nat. Commun.*, 2014, **5**, 5772.

22 H. Jin, C. L. Mangun, A. S. Griffin, J. S. Moore, N. R. Sottos and S. R. White, *Adv. Mater.*, 2014, **26**, 282–287.

23 V. Trappe, V. Prasad, L. Cipelletti, P. N. Segre and D. A. Weitz, *Nature*, 2001, **411**, 772–775.

24 M. I. Smith, R. Besseling, M. E. Cates and V. Bertola, *Nat. Commun.*, 2010, **1**, 114.

25 S. A. Odom, S. Chayanupatkul, B. J. Blaiszik, O. Zhao, A. C. Jackson, P. V. Braun, N. R. Sottos, S. R. White and J. S. Moore, *Adv. Mater.*, 2012, **24**, 2578–2581.

26 S. S. Lee, B. Kim, S. K. Kim, J. C. Won, Y. H. Kim and S.-H. Kim, *Adv. Mater.*, 2015, **27**, 627–633.

27 J. D. Rule, E. N. Brown, N. R. Sottos, S. R. White and J. S. Moore, *Adv. Mater.*, 2005, **17**, 205–208.

28 J. X. Ni, L. Song, Y. A. Hu, P. Zhang and W. Y. Xing, *Polym. Adv. Technol.*, 2009, **20**, 999–1005.

29 D. G. Shchukin, M. Zheludkevich, K. Yasakau, S. Lamaka, M. G. S. Ferreira and H. Möhwald, *Adv. Mater.*, 2006, **18**, 1672–1678.

30 J. J. Vericella, S. E. Baker, J. K. Stolaroff, E. B. Duoss, J. O. Hardin, J. Lewicki, E. Glogowski, W. C. Floyd, C. A. Valdez, W. L. Smith, J. H. Satcher, W. L. Bourcier, C. M. Spadaccini, J. A. Lewis and R. D. Aines, *Nat. Commun.*, 2015, **6**, 6124.

31 D. Sun, J. An, G. Wu and J. Yang, *J. Mater. Chem. A*, 2015, **3**, 4435–4444.

32 D. Sun, H. Zhang, X.-Z. Tang and J. Yang, *Polymer*, 2016, **91**, 33–40.

33 J. S. Drury, *J. Ind. Eng. Chem.*, 1952, **44**, 2744.

34 K. A. Dannemann and J. Lankford, *Mater. Sci. Eng., A*, 2000, **293**, 157–164.

35 K. Arakawa, *Sci. Rep.*, 2017, **7**, 40102.